Journal of Materials Chemistry C

PAPER

Determination of Ga auto-incorporation in nominal InAlN epilayers grown by MOCVD

Cite this: J. Mater. Chem. C, 2014, 2, 5787

M. D. Smith,[ab] E. Taylor,[c] T. C. Sadler,[ab] V. Z. Zubialevich,[ab] K. Lorenz,[d] H. N. Li,[ab] J. O'Connell,[e] E. Alves,[d] J. D. Holmes,[bef] R. W. Martin[c] and P. J. Parbrook*[ab]

Received 10th March 2014
Accepted 13th April 2014

DOI: 10.1039/c4tc00480a

www.rsc.org/MaterialsC

We report on the consistent measurement of gallium incorporation in nominal InAlN layers using various complimentary techniques, underpinned by X-ray diffraction. Nominal InAlN layers with similar growth conditions were prepared, and the change in unintended Ga content in the group III sublattice ranged from ~24% to ~12% when the total reactor flow rate was increased from 8000 to 24 000 standard cubic centimetres per minute. Ultra-thin InAlN/GaN HEMT layers were grown in a clean reactor to minimize Ga auto-incorporation, and measured using X-ray photoelectron spectroscopy and secondary ion mass spectrometry. The implications of Ga incorporation in InAlN layers within optoelectronic and power devices is discussed.

1. Introduction

InAlN is an attractive candidate to replace AlGaN and InGaN in optoelectronic[1,2] and power transistor[3,4] applications due to its ability to be lattice matched to GaN at ~17% indium content, where it has a large band gap and good thermo-chemical stability thanks to its similarity to AlN. InAlN layers and other III-nitride materials are commonly prepared by metalorganic chemical vapour deposition (MOCVD) where group III precursors, typically trimethylalkyls, react with NH_3 in carefully controlled conditions on a substrate surface, such as sapphire, silicon carbide or silicon. Recently it has been reported that unintentional Ga incorporation in InAlN layers can occur during MOCVD growth, attributed to both left-over Ga-containing residue from previous growth on the reactor walls/susceptor[5–9] or the decomposition of preceding Ga-containing layers.[10] Each proposed reason has convincing arguments, particularly when the geometry of the reactor and the use of Ga in the preparation of buffer or device layers prior to the InAlN growth are considered.

Unwanted Ga has implications for both the structural and electrical properties of InAl(Ga)N epilayers. The band gap and polarisation of the layer both depend on the composition fraction, and are critical parameters in determining the wavelength and efficiency of light emitted by an optoelectronic device and also the current handling capabilities of a power transistor. Structurally the growth mechanism of a quaternary epilayer may differ from that of a ternary, and as such the morphology of as-grown layers may not be the same. This is particularly important for heterostructures where interfacial roughness is a limiting factor, as for InAlN/GaN high electron mobility transistors (HEMTs).[11] MOVPE growth of InAlN/GaN heterostructures is a fundamental stage in achieving the desired electrical performance in InAlN HEMTs, and modifications to optimise growth and processing may not have the desired effect if implemented on InAlGaN layers.

2. Experimental procedure

Initially, three nominally InAlN (80 nm) layers were grown on 1 μm GaN buffer layers in a 3 × 2″ AIXTRON close coupled showerhead MOCVD reactor, on 0.4 degree miscut sapphire substrates. All layers were non-intentionally doped. All layers were grown continuously, and before each wafer was grown the showerhead through which precursor gases enter the reactor was cleaned and the reactor baked in an attempt to minimise contamination of epilayers. Trimethylgallium (TMGa), trimethylindium (TMIn) and trimethylaluminium (TMAl) were used as group III precursors and ammonia supplied the group V content with N_2 and H_2 used as carrier gases. The GaN layers used a standard recipe, with a low temperature GaN nucleation layer followed by growth at 1060 °C with H_2 used as a carrier gas. Afterwards the reactor conditions and carrier gases were changed to those suitable for InAlN growth, with N_2 carrier gas both for the main reactor flow and as the precursor flow for both TMAl and TMIn. The InAlN epilayer growth parameters for

[a]Tyndall National Institute, University College Cork, Lee Maltings, Dyke Parade, Cork, Ireland. E-mail: peter.parbrook@tyndall.ie
[b]School of Engineering, University College Cork, College Road, Cork, Ireland
[c]Department of Physics, SUPA, University of Strathclyde, Glasgow, G4 0NG, Scotland, UK
[d]IPFN, Instituto Superior Técnico, Campus Tecnológico e Nuclear, Universidade de Lisboa, Estrada Nacional 10, P-2695-066 Bobadela LRS, Portugal
[e]Department of Chemistry, University College Cork, College Road, Cork, Ireland
[f]Centre for Research on Adaptive Nanostructures and Nanodevices (CRANN), Trinity College Dublin, Dublin 2, Ireland

Table 1 Selected growth parameters for the nominally InAlN epilayers grown in this series (sccm is standard cubic centimetres per minute). Also shown are composition fraction results from WDX and RBS measurements, checked for consistency by XRD, and fitting parameters for XRD analysis. The linear fitting refers to the lines in Fig. 3, assuming fully strained InAlGaN on relaxed GaN

	Sample A	Sample B	Sample C
NH_3 (mmol min^{-1})	56	168	56
TMIn (μmol min^{-1})	5	16	5
TMAl (μmol min^{-1})	5	16	5
Growth time (s)	1330	1300	2520
Reactor total flow (sccm)	8000	24000	24000
WDX Al%	69.0	73.0	79.0
WDX In%	7.0	15.0	7.0
WDX Ga%	24.0	12.0	14.0
RBS Al%	72.2	74.9	79.7
RBS In%	7.9	14.4	8.0
RBS Ga%	19.9	10.7	12.3
XRD thickness (nm)	87.5	82.0	88.0
RBS thickness (nm)	80	79	81
Linear fitting			
'*m*' gradient value	−4.00	−4.05	−3.99
'*c*' intercept value	0.56	0.72	0.49
If layers were Ga-free: XRD composition estimate	Al: 86.0% In: 14.0%	Al: 82.2% In: 17.8%	Al: 87.8% In: 12.3%

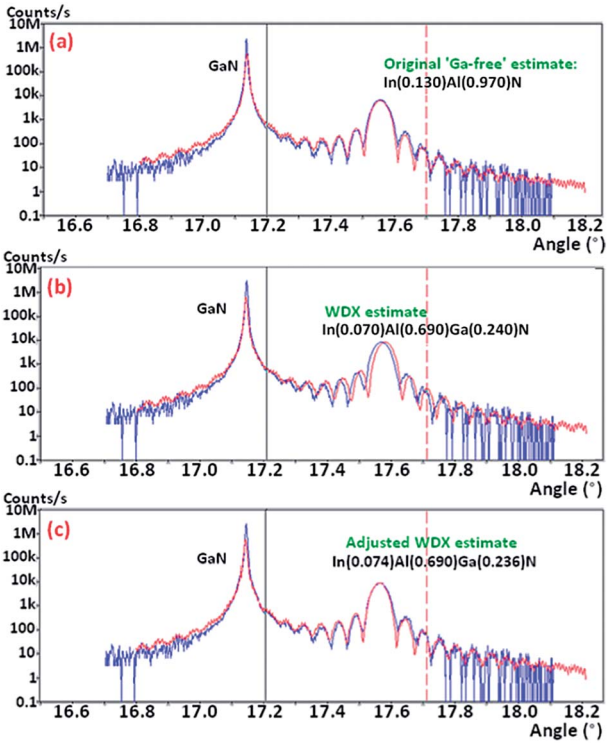

Fig. 1 ω–2θ (0002) XRD scans of sample A using a Ga-free InAlN layer (a), WDX composition values (b) and WDX values adjusted visually (c). This method is sensitive to changes in composition down to 0.1%.

samples A, B and C are presented in Table 1 below. The temperature, pressure and V/III ratio used were 790 °C, 70 mbar, and 5481, respectively in all cases.

Structures were analysed succeeding growth by X-ray Diffraction (XRD), using a PANalytical X'Pert double crystal diffractometer to make an ω–2θ 0002 scan and dynamical diffraction fitting software, allowing the InAlN *c*-plane lattice parameter to be measured, and the layer thickness calculated from the Pendellösung fringes. The measurement of thickness is generally very sensitive to the fringe spacing allowing an estimated error of ±1 nm. Assuming the layer to be both fully strained and Ga free an initial estimate of the InAlN composition was made, as shown in Fig. 1a. A (10-15) reciprocal space map suggested the InAlN layers to be fully strained to the GaN buffer, to within a relatively large experimental error of ~30%.

While the *c*-plane lattice parameter and knowledge of the strain state of a layer can give an accurate estimate of the composition of ternary compound such as InAlN, it cannot unequivocally estimate the composition of a quaternary like InAlGaN as for fully strained layers a range of compositions will allow fitting. Thus alternative methods are required: Wavelength Dispersive X-ray Spectroscopy (WDX)[12–16] determines a sample's atomic composition through X-ray fluorescence produced by exciting a constituent atom's inner shell electrons using a focused high energy electron beam. Rutherford Backscattering Spectrometry (RBS)[17–21] uses a positive ion beam scattering off the nuclei of a lattice's constituent atoms, and an analysis of the energy and angle of the redetected beam can generate a composition–depth profile. The RBS and WDX measurements exploit different fundamental properties of a lattice's constituent atoms, so the two may be considered independent of each other and the XRD measurement.

WDX and RBS are techniques that require layers thicker than those practical for use as III-nitride HEMT barrier layers for valid measurements, and other methods must be sought to confirm the presence of Ga for thinner layers. Three HEMT wafers were prepared, as shown in Fig. 2 – HEMT-1 and HEMT-2 were grown continuously with InAl(Ga)N barrier layer flow conditions identical to that of sample A described in Table 1, and have thicknesses of 9 nm and 14 nm respectively, on top of GaN buffer layers with 1 nm AlN interlayers.[11] For HEMT-3, a revised growth procedure was developed with the aim of eliminating Ga auto-incorporation in the ultra-thin barrier layer. A growth pause after GaN buffer layer deposition was included,

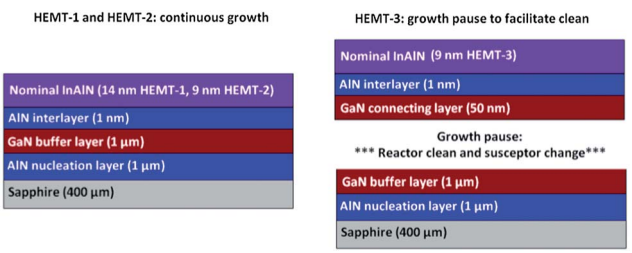

Fig. 2 Schematic of the HEMT layers grown in this series. HEMT-1 and HEMT-2 were grown continuously while HEMT-3 included a growth pause so the reactor could be cleaned and susceptor changed.

during which time the reactor & showerhead were cleaned and the susceptor changed to one not previously exposed to MOVPE of Ga-containing layers. Growth of the 9 nm InAlN barrier layer and AlN interlayer then commenced after deposition of a 50 nm GaN connecting layer, thought to be sufficiently thin to not influence the composition of the subsequent layer.

HEMT-1 and HEMT-3 were analysed by surface SIMS (secondary ion mass spectrometry), where a sample surface is sputtered with a focussed ion beam and the resulting ejected secondary ions are detected, providing a composition–depth profile. X-ray photoelectron spectroscopy (XPS) analysis was performed on HEMT-2 and HEMT-3: the technique exploits the process of X-ray fluorescence to determine the composition just a few nanometres into the surface. Despite care being taken to avoid Ga or Al signals from the buffer layers beneath the measured InAl(Ga)N layer being picked up (with the edge facing the incident X-ray beam covered by evaporated Au) the XPS measurement should still only be treated as a guide as further development and validation of accurate measurement is required.

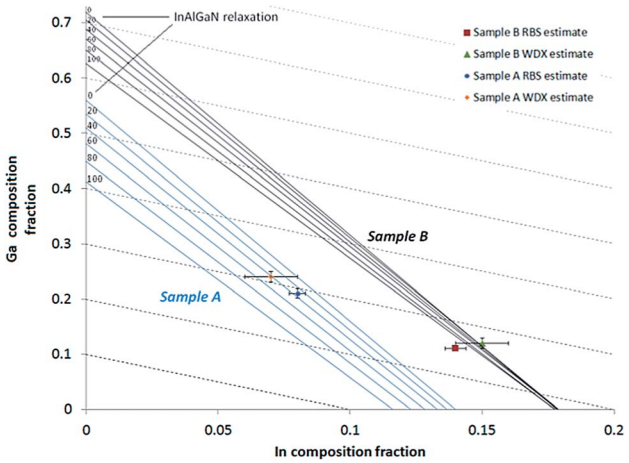

Fig. 3 [0002] ω–2θ XRD fitting parameters that give compatible results for sample A (solid blue lines) and sample B (solid black lines), with different InAl(Ga)N relaxation values considered. Constant Al content contour lines are also shown (dashed lines).

3. Results and discussion

a. Thick InAl(Ga)N layers

The compositional estimates for the samples A, B and C analysed are shown in Table 1. XRD indicated InAlN compositions in the range of 12–18% InN assuming the absence of gallium. As a test of the consistency of the measurement the WDX composition fraction estimates can be fed back into the XRD fitting software and the legitimacy of the measurement scrutinized. Fig. 1b exhibits the fit to the experimental curve data based on the WDX derived values, showing a close match. In this case, fixing the Al and modifying the In and Ga concentrations by less than 0.5% can lead to a fit (Fig. 1c) that is as good as the original fit assuming pure InAlN (Fig. 1a). Such a small change is well within the error limits of the WDX compositional measurement. Similarly, feeding the RBS composition fraction estimates back into the XRD simulation confirms a match that is self-consistent given the uncertainties in the measurement (detailed in ref. 22).

While the RBS data is consistent with films uniform in composition, this cannot be assumed the case given the source of the Ga in the "InAlN" films has not been unequivocally determined. It may be possible that the Ga content may have a graded profile, and indeed SIMS data suggests graded Al and Ga composition–depth profiles down the heterointerface (with In appearing to mediate the process by maintaining a constant composition fraction), with profiles becoming flat after ~4 nm. Further work is required to analyse this effect and further probe the origins of the phenomenon.

Fig. 3 exhibits the complete range of composition fractions that are compatible with the XRD (0002) scan for two samples (A and B). The lines produced were based on multiple simulations using the X'Pert X-ray fitting software to confirm the linear nature of the compositional XRD isolines. The range of compositions allowed by XRD assuming fully strained InAlGaN on relaxed GaN can be fitted by a line using the values in Table 1. It should be noted that the RBS and WDX data for sample A do not lie on the line representing a fully strained InAlGaN layer, and might suggest some limited InAlGaN relaxation (relative to the underlying GaN layer). With the exception of the WDX measurement of sample B, all the compositional analyses of the three samples indicated fell into this regime. Given the width of the peaks in Qx in reciprocal space it is possible that there is some limited relaxation, or development of relaxation across the 80 nm film towards the surface, though a relaxation as high as 30–40% seems unlikely. We believe the variances observed are related to the respective errors in the different techniques, and assume the layer to be close to fully strained whilst acknowledging a degree of uncertainty in this regard. In this analysis we also assume the >1 μm GaN layers grown on sapphire to have 100% relaxation, and would expect any residual strain in the GaN to have negligible second order effects on the data.

A significant proportion of gallium is found in all three samples, ranging from 11% (RBS estimate, sample B) to 24% (WDX estimate, sample A), clearly showing a consistent presence in all nominally Ga-free layers. This could be easily overlooked if a layer was grown and immediately characterised *via* XRD for a composition fraction estimate, as a pure InAlN layer might have the same *c*-plane lattice parameter as an InAlGaN layer. The subtle structural and electrical effect of Ga contamination may provide substantial problems when processing and characterizing a semiconductor device if a pure InAlN layer is assumed, for example when trying to optimise a contact to a HEMT, polarisation-match a quantum well or optimise the reflectivity of a distributed Bragg reflector (DBR).

Referring to Table 1 we can analyse the growth conditions used for the InAl(Ga)N layers of samples A, B and C and compare composition estimates to probe the origins of the Ga contamination. A reduced gallium content is seen for samples B and C compared with A. Referring again to Table 1 we see that an increase in the total gas flow into the reactor, that is the

combined flow of the N_2 carrier gases and TMAl and TMIn (but not TMGa), appears to suppress gallium incorporation in the upper layer. Sample B has three times the group III and V precursor flows of sample A, and the carrier flows are scaled up accordingly to give a total flow of 24 000 standard cubic centimetres per minute (sccm) compared to 8000 sccm for A. Sample C uses the same group III and V precursor flow rates as A but has the high 24 000 sccm total flow rate as used for sample B. The InAl(Ga)N thickness was maintained by extending the growth time.

It is clear that increasing the total flow rate from 8000 sccm to 24 000 sccm acts to suppress Ga incorporation in the InAl(Ga)N layers by ~50%. This suggests a higher gas flow prevents lingering contaminants from reacting on the surface of the wafer, supporting an argument[5–9] that unwanted Ga in the group III sublattice originates from Ga-containing material sticking to the reactor walls, susceptor and/or gas delivery pipes and partially redepositing on a wafer surface during subsequent growth runs.

The small measured difference in Ga fraction between layers B and C (with proportions spanning 11–14%) is much less than the higher values of ~25% Ga content obtained for sample A. Furthermore sample B contains roughly twice as much indium as sample C. This suggests the higher growth rate in sample B relative to sample C (arising due to the larger ratio of precursor gas flow to total gas flow) acts to reduce indium desorption, encouraging a more indium rich lattice than when the growth rate is lower as in sample C. This may give further clues as to the mechanisms at work during pure InAlN growth, although further analysis is required before a conclusion can be made.

To fully suppress Ga incorporation into InAlN-on-GaN layers the susceptor and glassware through which precursor gases are delivered may have to be cleaned, along with the reactor and showerhead itself, between GaN and InAlN growth. Over many growth runs matter builds up on the walls of the reactor over which it passes and there may be no way to prevent it redepositing by modulation of the gas flow and growth conditions alone. The geometry and design of the AIXTRON CCS system makes a full clean a long and cumbersome task, which may prevent it from being a practical solution. Instead it may be more useful to consider embracing a small, controllable amount of Ga and modifying MOCVD growth and device processing accordingly.

Ga incorporation in nominal InAlN layers has implications for all InAlN-based devices; although InAlGaN/AlN/GaN HEMTs have been reported with power handling capabilities and high frequency operation comparable with state-of-the-art InAlN and AlGaN based devices,[23] both growth and processing must be adjusted to facilitate the difference in structural and electrical properties and the composition fraction must be tightly controlled for performance to be optimised. From a HEMT reliability perspective InAlGaN layers can be grown lattice-matched to GaN, both reducing interfacial roughness scattering[23] and eliminating interfacial strain, a potential HEMT

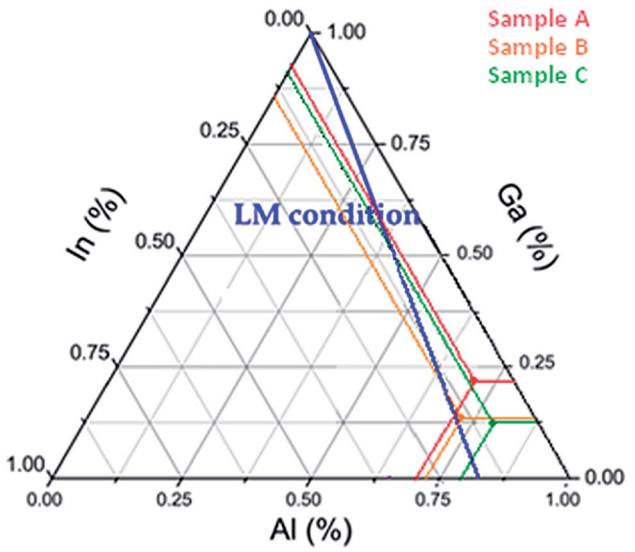

Fig. 4 Quaternary map of samples A, B and C, showing the compositions of InAlGaN lattice matched to GaN.

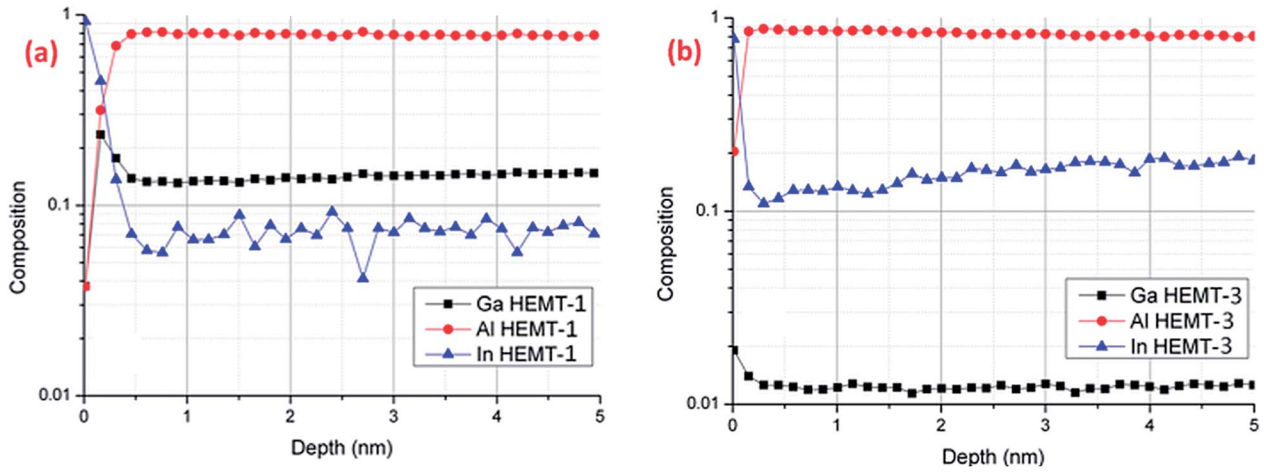

Fig. 5 SIMS profiling of InAlN HEMT barrier layers without (a) and with (b) the MOVPE reactor undergoing a clean and change in susceptor to one not previously exposed to Ga-containing layers (HEMT-1 and HEMT-3 respectively).

failure route when operated under extreme temperatures, radiation environments and current/voltage stressing. For optoelectronic devices InAlN can be used for bandgap engineering and polarisation matching in quantum well structures to optimise light output efficiency and a desired wavelength.[24] The graphic displayed in Fig. 4 is a quaternary map representing the composition of the InAlGaN layers grown in this work in comparison to that required to be lattice matched to GaN. Sample B lies close to the solid blue line, suggesting it has an in-plane lattice parameter identical to that of the underlying GaN layer and is thus fully relaxed/free of strain.

b. Ultra-thin InAl(Ga)N HEMT layers

The results of SIMS analysis on heterostructures HEMT-1, grown in the conventional manner without a growth pause and HEMT-3, grown with a pause during which the reactor was cleaned and susceptor changed, are displayed in Fig. 5 and summarised in Table 2. Removing the samples from the reactor before InAlN growth for InAlN-on-GaN heterojunction transistors and taking measures to minimise unintended Ga incorporation is found to suppress contamination by at least an order of magnitude, confirming the source to be residual matter inside the growth chamber and not inter-diffusion from the underlying buffer layer.[5–9]

Despite HEMT-1 and HEMT-2 being grown with nominally identical conditions as sample A (except for growth time), different composition values were measured. This is partly due to grading in the Al and Ga compositions at the heterointerface, which will contribute proportionally depending on the InAlGaN layer thickness, but may be chiefly attributed to the different, undefined measurement resolutions of the various techniques in the depth direction.

Table 2 Comparison of samples grown conventionally and using a revised growth procedure to suppress Ga auto-incorporation

Sample	In%	Ga%	Al%	Comment
HEMT-1	~8	~13	~79	No reactor conditioning
HEMT-3	~18	~1	~81	Reactor cleaned & susceptor changed before InAlN growth

Table 3 XPS results table corresponding to HEMT-2 and HEMT-3 as in Fig. 5

Name	Position (eV)	FWHM (eV)	Composition (%)
HEMT-2 Al – 2p	73.4	3.7	77
HEMT-2 Ga – 2p	1118.4	3.6	7
HEMT-2 In – 3d	444.8	4.2	16
HEMT-3 Al – 2p	73.6	3.3	80
HEMT-3 Ga – 2p	1118.6	3.4	1.2
HEMT-3 In – 3d	445.0	3.5	19

XPS is a cheaper, faster alternative to SIMS, which can be costly and time consuming. Results are shown in Fig. 6 and Table 3, where the binding energy position represents the species of atom detected (assuming certain information about the bonding state, which is valid here) and the area of the peak describes the abundance, once the X-ray sensitivity factors are accounted for. Table 3 indicates that HEMT-3, grown using the revised procedure aiming to suppress unwanted Ga incorporation in the nominally InAlN barrier layer, has 6 times less Ga in the region of crystal nearest the surface than the reference sample HEMT-2, grown under conditions favourable to Ga contamination to ensure it is detectable by the non-optimised XPS measurement. This qualitatively supports the SIMS data and the hypothesis that unwanted Ga in InAlN layers arrives from lingering precursors in the reactor during InAlN growth, especially given the fact that HEMT-3 shows only ~1% Ga contamination in both cases. Further development and validation of the XPS cross referenced with SIMS measurements will allow XPS to be used as a rapid robust feedback technique for ultra-thin InAlGaN HEMT layers, although more work is required to this end.

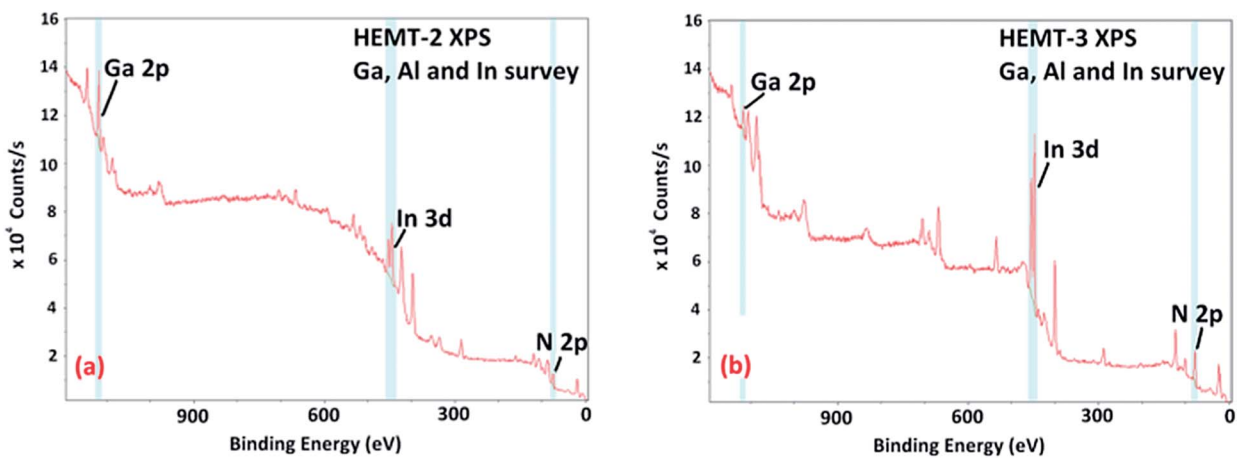

Fig. 6 XPS profiling of InAlN HEMT barrier layers without (a) and with (b) the MOVPE reactor undergoing a clean and change in susceptor to one not previously exposed to Ga-containing layers (HEMT-2 and HEMT-3 respectively).

4. Conclusion

Nominal InAlN layers were found to contain gallium at high group III sub-lattice fractions in the 12–24% range, depending on the growth conditions. RBS and WDX were used to measure composition fractions, supported by ω–2θ (0002) XRD scans, also used to confirm and refine the WDX and RBS data. The results suggest Ga incorporation may be suppressed by increasing the total gas flow into the reactor, indicating the origin of unwanted Ga is the susceptor and the walls of the reactor. Ultra-thin InAlN HEMT epilayers were analyzed using SIMS and XPS, and a revised InAlN HEMT growth procedure aimed at reducing Ga auto-incorporation was shown to be successful.

Acknowledgements

We are grateful to Andrew Barnes and Fabio Vitobello (both from ESTEC, European Space Agency) for useful discussion. We acknowledge funding from the UK Engineering and Physical Sciences Research Council (EPSRC, Grant numbers EP/I012591/1 and EP/I029141/1), European Space Agency (ESA) and Science Foundation Ireland (Grant no. 10\IN.1\I2993 and 07\EN\E001A). MDS and TCS acknowledge the Irish Research Council for their studentship and postdoctoral fellowship, respectively. MDS acknowledges studentship co-funding from ESA. This work was conducted under the framework of the Irish Government's Programme for Research in Third Level Institutions Cycle 4 and 5, National Development Plan 2007–2013 with the assistance of the European Regional Development Funds "INSPIRE" and "TYFFANI". We also thank FCT Portugal (grants PTDC/FIS-NAN/0973/2012 and "Investigador FCT") and SFI under grant code 09-IN.1-I2602.

Notes and references

1 G. Cywinski, C. Skierbiszewski, A. Fedunieiwcz-Zmuda and M. Siekacz, *J. Vac. Sci. Technol., B: Microelectron. Nanometer Struct.*, 2006, **24**(3), 1505–1509.
2 G. Naresh-Kumar, B. Hourahine, A. Vilalta-Clemente, P. Ruterana, P. Gamarra, C. Lacam, M. Tordjman, M. A. di Forte-Poisson, P. J. Parbrook, A. P. Day, G. England and C. Trager-Cowan, *Phys. Status Solidi A*, 2012, **209**(3), 424–426.
3 F. Lecourt, N. Ketteniss, H. Behmenburg, N. Defrance, V. Hoel, M. Eickelkamp, A. Vescan, C. Geisen, M. Heuken and J.-C. De Jaeger, *IEEE Electron Device Lett.*, 2011, **32**(11), 1537–1539.
4 M. Mikulics, R. Stoklas, A. Dadgar and D. Gregusova, *Appl. Phys. Lett.*, 2010, **97**(17), 173505.
5 S. Choi, H. J. Kim, Z. Lochner, J. Kim, R. D. Dupuis, A. M. Fischer, R. Juday, Y. Huang, T. Li, J. Y. Huang, F. A. Ponce and J.-H. Ryo, *J. Cryst. Growth*, 2014, **388**, 137–142.
6 J. Kim, Z. Lochner, M.-H. Ji, S. Choia, H. J. Kim, J. S. Kim, R. D. Dupuis, A. M. Fischer, R. Judayd, Y. Huangd, T. Lid, J. Y. Huangd, F. A. Ponced and J.-H. Ryoue, *J. Cryst. Growth*, 2014, **388**, 143–149.
7 M. Hiroki, N. Watanabe, N. Maeda, H. Yokoyama, K. Kumakura and H. Yamamoto, *Jpn. J. Appl. Phys.*, 2013, **52**, 04CF02.
8 J. Lu, Y.-L. Hu, D. F. Brown, F. Wu, S. Keller, J. S. Speck, S. P. DenBaars and U. K. Mishra, *Jpn. J. Appl. Phys.*, 2012, **51**, 115502.
9 M. Hiroki, Y. Odaa, N. Watanabe, N. Maeda, H. Yokoyama, K. Kumakura and H. Yamamoto, *J. Cryst. Growth*, 2013, **382**, 36–40.
10 J. J. Zhu, Y. M. Fan, H. Zhang, G. J. Lu, H. Wang, D. G. Zhao, D. S. Jiang, Z. S. Liu, S. M. Zhang, G. F. Chen, B. S. Zhang and H. Yang, *J. Cryst. Growth*, 2012, **348**, 25–30.
11 M. D. Smith, T. C. Sadler, H. Li, V. Z. Zubialevich and P. J. Parbrook, *Appl. Phys. Lett.*, 2013, **103**, 081602.
12 D. Henry, Louisiana State University and J. Goodge University of Minnesota-Duluth, Wavelength-Dispersive X-Ray Spectroscopy (WDS), Geochemical Instrumentation and Analysis 2013, http://serc.carleton.edu/research_education/geochemsheets/wds.html, accessed March 2014.
13 E. Taylor, F. Fang, F. Oehler, P. R. Edwards, M. J. Kappers, K. Lorenz, E. Alves, C. McAleese, C. J. Humphreys and R. W. Martin, *Semicond. Sci. Technol.*, 2013, **28**(6), 065011.
14 R. W. Martin, P. R. Edwards, K. P. O'Donnell, M. D. Dawson, C. W. Jeon, C. Liu, G. R. Rice and I. M. Watson, *Phys. Status Solidi A*, 2004, **201**(4), 665–672.
15 K. P. O'Donnell, I. Fernandez-Torrente, P. R. Edwards and R. W. Martin, *J. Cryst. Growth*, 2004, **269**(1), 100–105.
16 D. Amabile, R. W. Martin, T. Wang, M. A. Whitehead and P. J. Parbrook, *Phys. Status Solidi C*, 2003, **0**(7), 2478–2481.
17 S. Magalhães, N. P. Barradas, E. Alves, I. M. Watson and K. Lorenz, *Nucl. Instrum. Methods Phys. Res., Sect. B*, 2012, **273**(0), 105–108.
18 N. P. Barradas, C. Jeynes and R. P. Webb, *Appl. Phys. Lett.*, 1997, **71**(2), 291–293.
19 K. Lorenz, N. Franco, E. Alves, I. M. Watson, R. W. Martin and K. P. O'Donnell, *Phys. Rev. Lett.*, 2006, **97**, 085501.
20 N. P. Barradas and M. A. Reis, *X-Ray Spectrom.*, 2006, **35**(4), 232–237.
21 C. Jeynes, Z. H. Jafri, R. P. Webb, A. C. Kimber and M. J. Ashwi, *Surf. Interface Anal.*, 1997, **25**(4), 254–260.
22 E. Taylor, M. D. Smith, T. C. Sadler, K. Lorenz, H. N. Li, P. J. Parbrook and R. W. Martin, *J. Appl. Phys.*, submitted.
23 G. L. Ronghua Wang, G. Karbasian, J. Guo, B. Song, Y. Yue, Z. Hu, O. Laboutin, Y. Cao, W. Johnson, G. Snider, P. Fay, D. Jena and H. G. Xing, *IEEE Electron Device Lett.*, 2013, **34**(3), 378–380.
24 P. Pampili, V. Z. Zubialevich, S. N. Alam, S. Schulz, M. A. Caro, E. P. O'Reilly and P. J. Parbrook, *Polarization-matched Active Region as a Way to Reduce Quantum Confined Stark Effect in a Near-UV LED, Poster Presentation at the UK Nitrides Consortium Annual Meeting Bristol*, 2014.

